Article

Activity of phosphatase-sensitive 5-aminolevulinic acid prodrugs in cancer cell lines

HERCEG, Viktorija, *et al*.

Abstract

5-aminolevulinc acid (5-ALA)-based photodynamic therapy (PDT) and photodiagnosis (PD) present many advantages over treatments with conventional photosensitizers (PS). It offers great tumor specificity, reduced photosensitivity reactions caused by PS accumulation in non-targeted tissues and also inherent PS metabolism into endogenous non-fluorescent heme. However, chemical instability, low bioavailability and poor pharmacokinetic profile limit systemic efficacy of 5-ALA. Here, we present a comprehensive in vitro evaluation of novel phosphatase-sensitive prodrugs of 5-ALA. These prodrugs are designed to be activated by ubiquitously expressed phosphatases with much improved chemical stability and reduced acute toxicity profile. PpIX kinetic measurements and flow cytometry show accumulation of PpIX upon incubation with phosphatase-sensitive prodrugs in PC3 human prostate cell cancer, MCF7 breast adenocarcinoma, U87MG glioblastoma, T24 bladder cancer and A549 lung carcinoma cells. They revealed a different fluorescence kinetics and dose-response curves for the different types of 5-ALA prodrugs. These experiments have allowed [...]

Reference

HERCEG, Viktorija, *et al*. Activity of phosphatase-sensitive 5-aminolevulinic acid prodrugs in cancer cell lines. *Journal of Photochemistry and Photobiology. B, Biology*, 2017, vol. 171, p. 34-42

DOI : 10.1016/j.jphotobiol.2017.04.029
PMID : 28472723

Activity of phosphatase-sensitive 5-aminolevulinic acid prodrugs in cancer cell lines

*Viktorija Herceg, Norbert Lange, Eric Allémann, Andrej Babič**

School of Pharmaceutical Sciences, University of Geneva, University of Lausanne, 1211, Geneva, Switzerland

Keywords

5-aminolevulinic acid, prodrugs, fluorescence, photodetection, photodynamic therapy

Abstract

5-aminolevulinc acid (5-ALA)-based photodynamic therapy (PDT) and photodiagnosis (PD) present many advantages over treatments with conventional photosensitizers (PS). It offers great tumor specificity, reduced photosensitivity reactions caused by PS accumulation in non-targeted tissues and also inherent PS metabolism into endogenous non-fluorescent heme. However, chemical instability, low bioavailability and poor pharmacokinetic profile limit systemic efficacy of 5-ALA. Here, we present a comprehensive in vitro evaluation of novel phosphatase-sensitive prodrugs of 5-ALA. These prodrugs are designed to be activated by ubiquitously expressed phosphatases with much improved chemical stability and reduced acute toxicity profile. PpIX

kinetic measurements and flow cytometry show accumulation of PpIX upon incubation with phosphatase-sensitive prodrugs in PC3 human prostate cell cancer, MCF7 breast adenocarcinoma, U87MG glioblastoma, T24 bladder cancer and A549 lung carcinoma cells. They revealed a different fluorescence kinetics and dose-response curves for the different types of 5-ALA prodrugs. These experiments have allowed us to identify the most promising cancer cell types for phospho- 5-ALA prodrugs. Confocal fluorescence microscopy provided further evidence of fluorescent protoporphyrin IX accumulation and sub-cellular localisation. These findings, together with the low toxicity profile of phosphatase-sensitive prodrugs of 5-ALA and good response to PDT provide solid basis for future translational development in PC3, MCF7 and U87MG cancer types.

Introduction

Photodynamic therapy (PDT) is a treatment modality in which a photosensitizer (PS), light, and oxygen are used to produce reactive oxygen species (ROS). ROS can cause damage to different cell organelles which ultimately leads to cell death. Furthermore, the intrinsic fluorescence of PSs can be used for photodetection (PD).

5-aminolevulinic acid (5-ALA) is a natural precursor of heme in heme biosynthesis that takes part partially in mitochondria and partially in the cytosol in nearly all cells containing a nucleus (Figure 1). In malignant cells, the exogenous administration of 5-ALA causes the temporary accumulation of a natural PS protoporphyrin IX (PpIX) due to the bypass of the feedback control mechanism governed by the free heme. This can be ascribed to altered activities of the enzymes involved in heme biosynthesis.[1-3] The endogenously produced PpIX is nowadays efficiently exploited in 5-ALA-mediated PDT and PD.

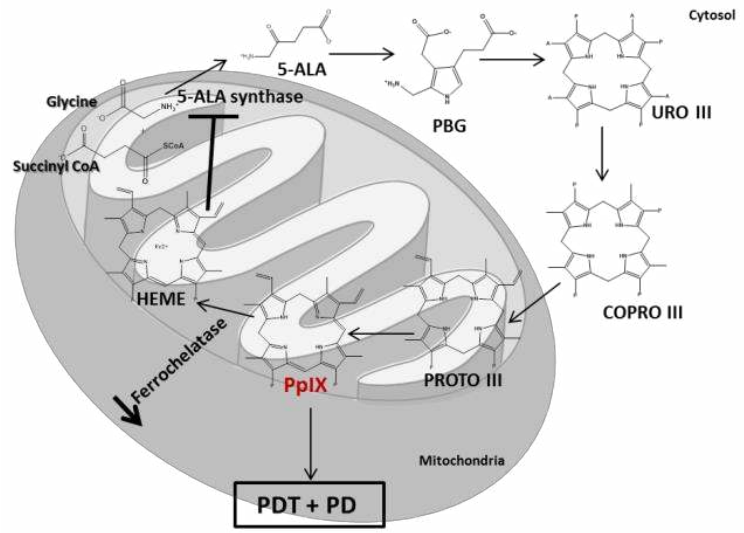

Figure 1. Schematic representation of the heme biosynthesis. Porphobilinogen (PBG), uroporphobilinogen III (URO III), coproporphyrinogen III (COPRO III), protoporphyrinogen III (PROTO III), protoporphyrin IX (PpIX).

5-ALA PDT demonstrates many advantages over PDT performed with conventional PS. Since 5-ALA does not possess properties of a PS, its administration does not provoke major photosensitivity reactions caused by PS accumulation in non-targeted tissues hence providing the possibility of repeated administration with reduced side effects. Moreover, PpIX produced after the administration of 5-ALA may be used not only for PDT, but also for diagnostic purposes to identify the early changes in tissues by means of fluorescence PD. During surgery, PD allows the identification and resection of very small lesions which are usually missed by conventional naked-eye examination.[4] Although primary employed in the treatment of dermatological conditions like actinic keratosis (AK), psoriasis, basal cell carcinoma, squamous cell carcinoma and Bowen's disease, 5-ALA has been tested for the treatment or detection of different malignancies ranging from brain tumors to lung cancer.[5, 6] Today, 5-ALA has been granted marketing authorization for

the treatment of AK[7-10] and the fluorescence-guided resection of malignant glioma.[4, 11, 12] Although showing promise for PDT and PD, 5-ALA has certain drawbacks when it comes to its physico-chemical properties. Being a charged zwitterion under physiological conditions, 5-ALA cannot efficiently pass biological barriers. Its limited bioavailability and poor pharmacokinetic profile make 5-ALA suboptimal for systemic administration.[13]

To overcome these shortcomings, different strategies have been employed. Up to now, making the molecule more lipophilic by esterification of its carboxyl function has provided the most effective solution reducing the dose needed for the optimal PpIX production up to 150-fold.[14] Nowadays, 5-ALA-methyl ester (Metvix®)[15] is granted use for the treatment of AK and basal cell carcinoma and 5-ALA-hexyl ester (ALA-Hex, Hexvix®) for the detection of bladder cancer.[16-19] Albeit improved in the terms of lipophilicity, ALA-Hex remains toxic with a poor systemic pharmacokinetic profile thus still not providing an optimal solution for the systemic administration.[20]

In order to circumvent the problem of poor drug-like properties of 5-ALA and its esters, we recently reported new 5-ALA prodrugs where the amino group of ALA-Hex was modified with a phosphatase-sensitive linker.[21] The presence of phosphatase activity in various tissues and their upregulated expression in certain types of cancer might provide a solution for a broader clinical application of 5-ALA PDT and PD.[22-25]

Phospho-self-immolative 5-ALA (PSI-ALA-Hex) and phospho-5-ALA (P-ALA-Hex) keep the lipophilicity of ALA-Hex which facilitates their uptake into cells compared to 5-ALA while having reduced acute toxicity and improved stability over a wide range of pH values. In addition, their activation and conversion to 5-ALA is controlled and can be tailored with changes to chemical structure (Figure 2).

In this work we present comprehensive *in vitro* evaluation of phosphatase-sensitive prodrugs of 5-ALA in five human cancer cell lines; human bladder carcinoma cell line T24, human lung adenocarcinoma cell line A549, human glioblastoma cell line U87MG, human breast adenocarcinoma cell line MCF7, and human prostate cancer cells PC3. To assess the pharmacological efficacy profile of new prodrugs, we compared the PpIX production in above mentioned cells, evaluated the dark- and photo- toxic effects upon exposure to different light doses and investigated the intracellular distribution and accumulation of PpIX by means of confocal fluorescence microscopy.

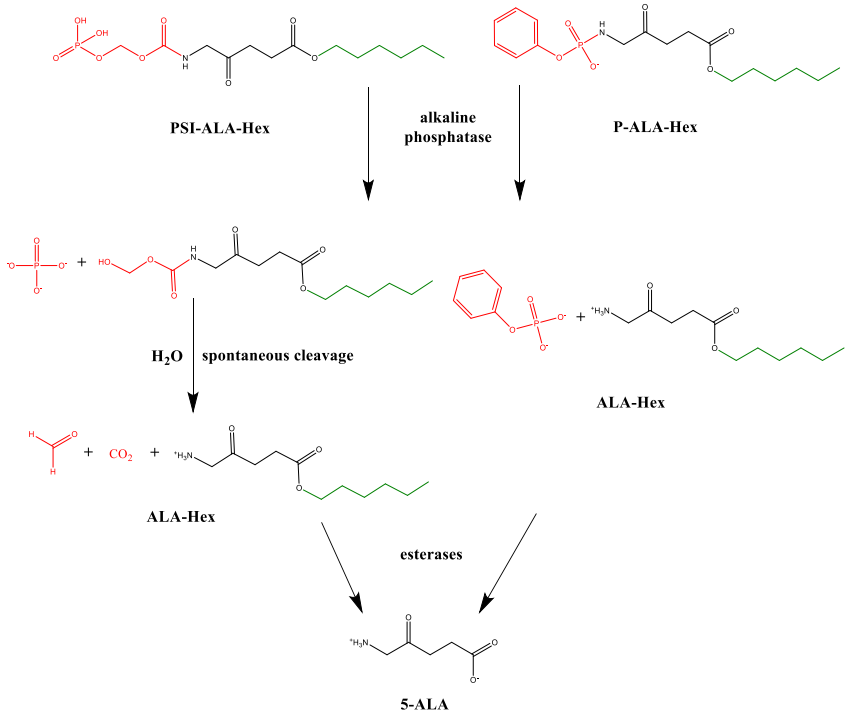

Figure 2. Activation of phosphatase-sensitive prodrugs PSI-ALA-Hex and P-ALA-Hex.

Materials and methods

Chemistry

The compounds PSI-ALA-Hex, P-ALA-Hex and ALA-Hex were synthesized according to published procedure.[21] The compounds were stored at -25 °C and dissolved in cell media before the experiments.

PSI-ALA-Hex: ^{1}H NMR (300 MHz, CD_3OD) δ 5.49 (d, *J* = 12.6 Hz, 2H), 4.17 – 3.96 (m, 4H), 3.17 (q, *J* = 7.3 Hz, 6H), 2.75 (t, *J* = 6.3 Hz, 2H), 2.57 (t, *J* = 6.3 Hz, 2H), 1.61 – 1.58 (m, 2H), 1.45 – 1.17 (m, 15H), 0.99 – 0.81 (m, 3H). ^{13}C NMR (75 MHz, CD_3OD) δ 205.49, 173.20, 156.52, 83.39, 83.33, 64.66, 49.73, 48.69, 48.41, 48.12, 47.84, 47.56, 47.27, 46.99, 46.28, 33.82, 31.43, 28.49, 27.48, 25.51, 22.44, 13.20, 7.93. LRMS: m/z 368.0 $[M-H]^-$, 737.3 $[2M-H]^-$, 1106.7 $[3M-H]^-$. HRMS: m/z calculated for C13H23NO9P 368.1116 $[M-H]^-$, observed 368.1115.

P-ALA-Hex: ^{1}H NMR (300 MHz, CD3OD) δ 7.34 – 7.14 (m, 4H), 7.11 – 6.96 (m, 1H), 4.02 (t, J = 6.6 Hz, 2H), 3.82 (d, J = 8.3 Hz, 2H), 3.18 (q, J = 7.3 H, 6H), 2.73 (dd, J = 7.2, 5.6 Hz, 2H), 2.53 (dd, J = 7.2, 5.5 Hz, 2H), 1.67 – 1.48 (m, 2H), 1.31 (m, 17H), 0.96 – 0.84 (m, 3H). ^{13}C NMR (75 MHz, CD3OD) δ 208.05 (d), 173.34, 153.34 (d), 129.12, 123.01, 120.66, 120.60, 64.66, 51.41, 48.77, 46.58, 33.94, 31.44, 28.51, 27.64, 25.52, 22.46, 13.30, 8.12. LRMS, ESI: m/z 370.4 [M-H], 741.5 $[2M-H]^-$, 1112.7 $[3M-H]^-$, 372.4 $[M+H]^+$, 743.7 $[2M+H]^+$, 1114.8 $[3M+H]^+$. HRMS: m/z calculated for C17H26NO6P 372.1571 $[M+H]^+$, observed 372.1573.

Cell culture

Human bladder carcinoma cell line T24 (ATTC® HTB-4™, Manassas, Virginia), human lung adenocarcinoma cell line A549 (ATTC® CCL-185™, Manassas, Virginia), human glioblastoma cell line U87MG (ATTC® HTB-14™, Manassas, Virginia), human breast adenocarcinoma cell

line MCF7 (ATTC® HTB-22™, Manassas, Virginia) and human prostate cancer cell line PC3 (ATTC® CRL-1435™, Manassas, Virginia) were grown as monolayers. Cells were maintained in DMEM+GlutaMAX™-I medium (T24 and A549), MEM (U87MG and MCF7) and F12K nutrient mix (PC3). Culture media were supplemented with 10 % fetal calf serum (CVFSVF00-01, Eurobio) and 100 µl/ml streptomycin and 100 IU/ml penicillin (15140-122, Thermo Fisher Scientific). Cells were cultivated at 37 ^{0}C in humidified 95 % air and 5 % CO_2 atmosphere and routinely maintained by serial passage into a new medium. All cell lines were tested for mycoplasma contamination with MycoAlert™ kit (LT07-418, Lonza) prior to experiments.

PpIX fluorescence measurements

Cells were plated in different densities according to their growth rate. T24 (5000 cells/well), PC3 (12000 cells/well), A549 (10000 cells/well), U87MG (10000 cells/well) and MCF7 (10000 cells/well) were seeded in a 96-well plate (clear bottom black plate, 3603, Corning) one day prior to the experiment. For experiments, complete medium was replaced with serum-free medium containing increasing concentrations (0.03, 0.10, 0.33, and 1.00 mM) of PSI-ALA-Hex, P-ALA-Hex and ALA-Hex. The PpIX fluorescence was recorded with a plate reader (Safire, Tecan, Switzerland) at different time points (1, 2, 4, 6, 8 and 24 h). Excitation wavelength was set at 405 nm and emission wavelength at 630 nm. For each experiment, raw data values obtained for the PpIX fluorescence measurements were corrected by subtraction of blank values (serum-free cell medium, depending on cell type). Mean values and s.d. from for each concentration per plate were calculated and plotted for each cell. All figures were generated using GraphPad Prism 6 software. P-value < 0.05 was considered as statistically significant.

Comparison of PpIX production in cells by flow cytometry

Cells (PC3, MCF7, T24 and A549) were seeded in 6 well plates (flat bottom cell culture microplate, 3505, Corning) and left to attach overnight. The next day, media was aspired and cells were treated with serum-free medium containing 0.33 mM of PSI-ALA-Hex, P-ALA-Hex and ALA-Hex. After 4 h of incubation in the dark at 37°C, cells were washed with DPBS and resuspended in DPBS. PpIX production in cells was assessed using BD LSRFortessa™ cell analyzer (BD Biosciences, Franklin Lakes, New Jersey). Excitation wavelength was set at 405 nm and emission filter used was 610 ± 20 nm.

Dark- and Phototoxicity

Upon 24 hours of incubation with PSI-ALA-Hex, P-ALA-Hex or ALA-Hex, cells were washed with DPBS and fresh complete medium was put into each well. LumiSource® (PCI Biotech, Oslo, Norway) provided a homogeneous blue light for the PDT. Cells were either irradiated with light dose of 1.4, 7.1 or 14.3 J/cm^2 or kept in the dark. Cell proliferation assays were performed 24 hours upon PDT treatment using a Cell Proliferation reagent (WST-1) (11644807001, Roche). The absorption was measured at 450 nm with a plate reader (Safire, Tecan, Switzerland). The percentage of cell survival was calculated with respect to control samples treated with either medium or a solution of DMSO (50 %) in serum-free medium, as follows: [A (test-conc.) - A (100 % dead) / A (100% viable) - A (100 % dead)] *100. Mean values from three wells were determined and expressed as +/- s.d.

Subcellular localization of PpIX in cancer cells

Human prostate cancer cells PC3 and breast adenocarcinoma MCF7 cells were seeded into ibidi µ-Slides, ibiTreat, 4 (80426-IBI) or 8 (80826-IBI) wells 24 h before the experiment. In order to investigate the subcellular distribution of PpIX, cell monolayers were incubated during different time periods in the dark at 37°C with 0.33 mM PSI-ALA-Hex, P-ALA-Hex and HAL in serum-free medium. Control cells were incubated in serum-free medium under the same experimental conditions. Cells were then washed with DPBS and incubated for another half hour with 1 µg/mL Hoechst 33342 stain (62249, Thermo Fisher Scientific) and 50 nM MitoTracker® Green FM (M7514 Thermo Fisher Scientific) or 70 nM of LysoTracker® Green DND-26 (8783 Thermo Fisher Scientific). Prior to imaging, cells were washed with DPBS and put in serum-free medium. Detection and localization of PpIX fluorescence in cells was done with the Zeiss LSM780 (Jena, Germany) inverted confocal microscope. The microscopic images were taken using 405 nm and 488 nm excitation lasers and 415 – 486 nm, 499 – 561 nm and 615 – 695 nm emission band filters, an objective lens Plan-Aprochromat 63 x/1.4 oil DIC M27. During the image acquisition time, slides were kept at 37°C in a humidified chamber (INUBTF-WSKM-F1, Tokai Hit, Gendoji-cho, Fujinomiya-shi, Shizuoka-ken, Japan). ZEN 2 software (Zeiss, Jena, Germany) was used for image processing. The quantification of co-localization between PpIX (red) and MitoTracker® Green FM or LysoTracker® Green DND-26 was done by calculating Pearson's coefficient of correlation (PCC) with Imaris x 64 8.0.0 software. PCC values may range between +1 (perfect correlation) and -1 (perfect negative correlation), where 0 means no correlation [26]. PCC was calculated in defined regions of interest (ROI). ROI was defined for each image separately by masking the dataset with red channel (PpIX fluorescence). The value of PCC for each experiment is presented as means ± s.d. calculated from 3 separate images.

Results

Influence of different 5-ALA derivatives on PpIX production

Time-dependent PpIX production was evaluated over 24 h in PC3 human prostate cancer, MCF7 breast adenocarcinoma, U87MG glioblastoma, T24 bladder carcinoma and A549 lung adenocarcinoma cells exposed to PSI-ALA-Hex, P-ALA-Hex and ALA-Hex at concentrations ranging from 0.03 mM to 1.00 mM. Higher prodrug concentrations (2.00 mM and 3.30 mM) were also tested initially (results not shown), but due to the cytotoxicity in the case of PSI-ALA-Hex and ALA-Hex, it was decided that the concentrations up to 1.00 mM would be used for further *in vitro* experiments.

Figure 3 shows the PpIX production in PC3 human prostate cancer cells continuously exposed to increasing concentrations of phosphatase-sensitive prodrugs or ALA-Hex for 24 h. PpIX fluorescence increased constantly over 24 h for all tested concentrations of PSI-ALA-Hex with its highest intensity achieved at 0.33 mM of prodrug concentration. On the other hand, for P-ALA-Hex, lower prodrug concentrations did not efficiently induce the synthesis of significant amounts of PpIX. However, at 1.00 mM of P-ALA-Hex constant increase in PpIX fluorescence was observed. ALA-Hex curves were similar to ones obtained with PSI-ALA-Hex except for the lowest concentration in which a plateau was reached after 8 h.

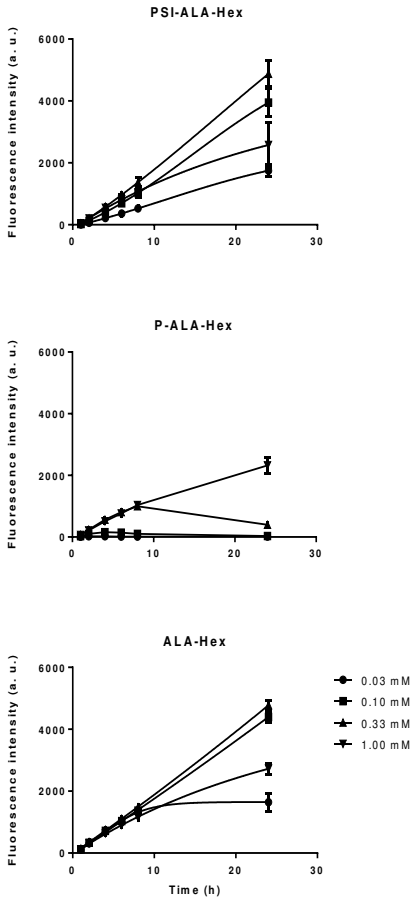

Figure 3. PpIX production measurements over 24 h in PC3 cells incubated with 0.03, 0.10, 0.33 and 1.00 mM PSI-ALA-Hex, P-ALA-Hex and ALA-Hex.

PpIX accumulation is depicted in Figure 4 as a function of prodrug concentration after 4 h in five different cancer cell lines. PpIX production was induced in all cells upon exposure to phosphatase-sensitive prodrugs of 5-ALA or ALA-Hex. However, important differences in PpIX production could be observed between different cancer cell lines. Generally speaking, PSI-ALA-Hex or ALA-Hex gave similar shaped dose-response curves. The highest PpIX production was seen in PC3 cells exposed to 0.33 mM of PSI-ALA-Hex or ALA-Hex (Figure 3, 4 and S1). Overall,

while optimal concentration of PSI-ALA-Hex varied between 0.03 and 0.33 mM depending on the cell type, P-ALA-Hex had a tendency to induce more PpIX production at higher concentrations. When exposed to phosphatase-sensitive prodrugs, PC3, MCF7 and U87MG cells showed PpIX production levels comparable to ones induced with ALA-Hex. As a result of these experiments, a 0.33 mM concentration of phosphatase-sensitive 5-ALA derivatives and ALA-Hex was chosen for comparison between different cell lines.

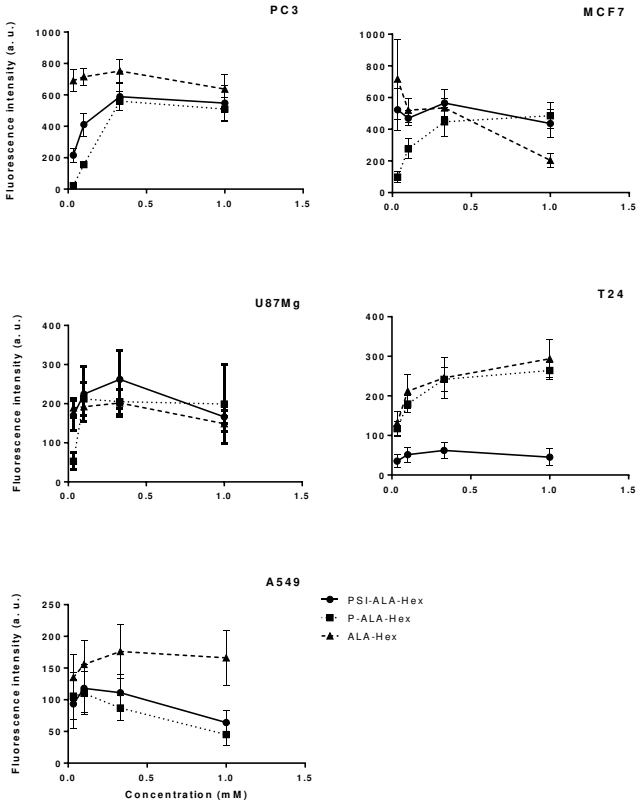

Figure 4. PpIX production after 4 h and as a function of concentration in five different cancer cell lines incubated with PSI-ALA (circles), P-ALA (squares) and ALA-Hex (triangles).

Since the cells were initially plated at different densities, PpIX production was additionally evaluated by means of flow cytometry to gain insight into the amount of PpIX produced per cell (Figure S2). For this purpose, cells were incubated for 4 h with 0.33 mM of PSI-ALA-Hex, P-ALA-Hex or ALA-Hex. Results of flow cytometry supported previously observed phenomena (Figure S2). PC3 cells showed the highest PpIX production per cell, followed by the MCF7. Again, in both of these cell lines, the amount of PpIX synthesized from phosphatase-sensitive prodrugs was comparable to ALA-Hex. T24 and A549 produce less PpIX compared to the other cancer cells.

Dark- and photo-toxicity

No dark toxicity was observed for the tested concentrations of phosphatase-sensitive prodrug of 5-ALA, P-ALA-Hex in all cell lines incubated with the product in the dark for 24 h (Figure S3). In the case PSI-ALA-Hex, its dark-toxicity depends on the cell type. While no dark-toxicity can be seen in PC3 and A549 cells, PSI-ALA-Hex shows some cytotoxicity at 1.00 mM concentration after 24 h incubation with MCF7 and T24 cell lines. No significant difference between PSI-ALA-Hex, P-ALA-Hex and ALA-Hex was observed in PC3 and MCF7 cells.

Cell proliferation following PDT (Figure S4) is shown for the optimal prodrug concentration for each cell line. Total death was reached after the exposure of PC3 and MCF7 cells to a light dose of 1.4 J/cm^2. For the A549 and T24 cells, much higher light doses were needed in order to observe a cytotoxic effect, 7.4 J/cm^2 and 14.1 J/cm^2, respectively. These results correlate with the lower amounts of PpIX produced in these two cell lines.

Subcellular localization of PpIX

Since the highest amounts of PpIX were produced in the MCF7 human breast adenocarcinoma and PC3 prostate cancer cells upon exposure to phosphatase-sensitive prodrugs and ALA-Hex, these two cell lines were chosen as model cells for the subcellular localization of PpIX.

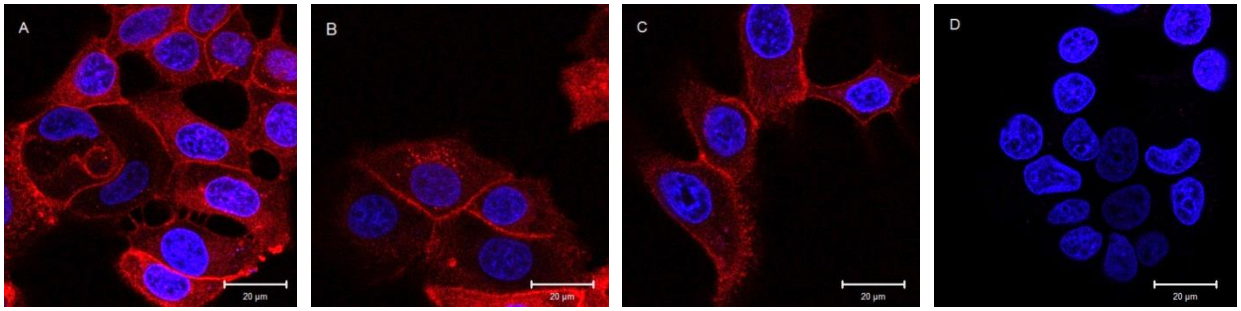

Figure 5. MCF7 confocal fluorescence micrographs upon 4 h incubation with 0.33 mM (a) PSI-ALA-Hex, (b) P-ALA-Hex and (c) ALA-Hex, (d) no treatment. Hoechst 33342 was used to label the cell nuclei in blue. PpIX fluorescence is shown in red. Magnification 63 x/immersion oil. Scale bar 20 µm.

Live imaging of MCF7 cells was performed to monitor the PpIX fluorescence with 0.33 mM of PSI-ALA-Hex, P-ALA-Hex and ALA-Hex. Fluorescence confocal images were taken at 2 h, 4 h and 8 h (Figures S5, S6, S7 and S8). In order to determine the localization of PpIX, MitoTracker® Green FM was used to label the mitochondria. Results of PpIX accumulation in MCF7 upon the incubation with PSI-ALA-Hex and ALA-Hex were compared with another cell line, PC3 (Figures S9, S10 and S11).

In MCF7 cells, PpIX induced fluorescence upon the incubation with PSI-ALA-Hex, P-ALA-Hex and ALA-Hex was initially dispersed throughout the cytoplasm. At 2 h, the calculated PCC between PpIX and the MitoTracker® Green, in the cells incubated with PSI-ALA-Hex, is

0.14±0.05. Figure 5 shows PpIX fluorescence at 4 h. PpIX was observed from well-defined regions in the cytoplasm as reported by others [14]. Accumulation of PpIX in the plasma membrane was also observed. Well-defined spots of PpIX emitted fluorescence seem to be situated closer to the cell nuclei at 8 h. Since there was no significant difference observed between PCC values from 2 h to 8 h in MCF7 cells, or between PSI-ALA-Hex, P-ALA-Hex and ALA-Hex, lysosomes were labeled in cells treated with PSI-ALA-Hex at 8 h with LysoTracker® Green to find out if PpIX fluorescence correlates with lysosomes (Figure 6).

In the case of PC3 cells (Figures S8, S9 and S10), at 2 h, PpIX fluorescence was dispersed throughout the cytoplasm, but significantly higher coefficient of correlation, 0.42±0.03, was calculated between PpIX and MitoTracker® Green than in MCF7 cells. PCC does not change at 4 h, but slightly increases to 0.51±0.03 at 8 h. The calculated correlation between PpIX and LysoTracker® Green in PC3 cells at 8 h is 0.26±0.03 vs 0.24±0.04 calculated for MCF7 cells (Tables S1 and S2) indicating that in these two cell lines only a minor part of PpIX colocalizes with lysosomes (Figure 6). Well-defined spots of PpIX fluorescence observed in MCF7 cells seem not to be present in PC3 cell line.

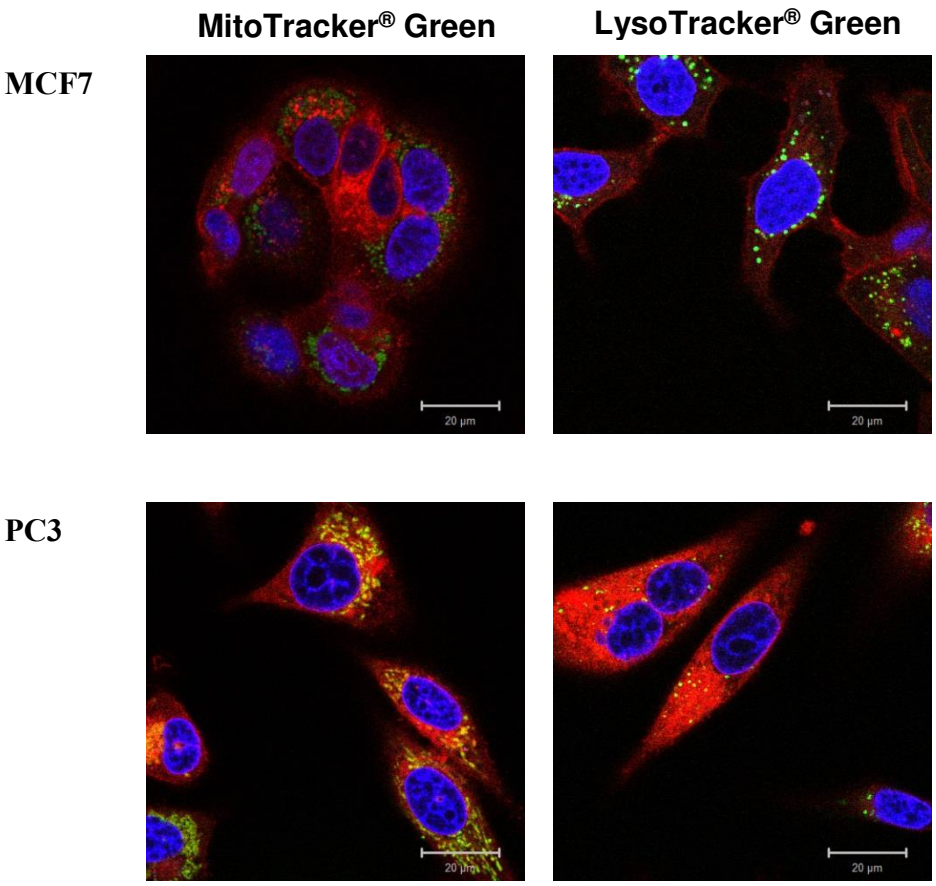

Figure 6. MCF7 and PC3 confocal fluorescence images after 8 h incubation with 0.33 mM PSI-ALA-Hex. PpIX fluorescence is represented in red. Mitochondria were labeled with MitoTracker® Green FM and LysoTracker® Green DND-26 was used for lysosome labelling. Yellow color presents the colocalization between PpIX and MitoTracker® Green FM or LysoTracker® Green DND-26. Magnification 63 x/immersion oil. Scale bar 20 µm.

Discussion

Major efforts have been undertaken to find the optimal strategy for the systemic delivery of 5-ALA. Best clinical outcome is reached when optimal equilibrium between molecule's ability to pass biological barriers, cell entry, PpIX induction and low toxicity is achieved. Under physiological pH found in the systemic circulation, 5-ALA is a zwitterion which greatly impairs its ability to pass biological barriers. Despite the fact that many different strategies have been employed in order to tackle this problem, up to date, the best option remains to be the esterification of 5-ALA carboxylic function. A plethora of 5-ALA esters has been reported with the improved lipophilicity and cell uptake.[27, 28] However, most of these molecules still remain considerably toxic and therefore not suitable for systemic administration [13, 20]. Furthermore, the unprotected 5-amino group makes the molecule chemically unstable at physiological pH found in bloodstream leading to its degradation and irreversible formation of cyclic dimers that are not able to enter the heme cycle.[29, 30] Although different strategies have been employed in order to protect the 5-amino group of 5-ALA while keeping some pharmacological activity, they did not really provide any promising candidates for further development.[31, 32]

Our approach to protect the amino group in 5-ALA from degradation by integration of phosphatase-sensitive moieties aims at providing the stability needed for the systemic administration of 5-ALA whilst keeping the toxicity profile low. As it was previously reported, both protease-sensitive prodrugs are better tolerated in chick embryos than ALA-Hex. Moreover, the acute *in vivo* toxicity studies showed a 5-fold increase in the tolerated dose of P-ALA-Hex compared to ALA-Hex.[21]

In this study we compared PSI-ALA-Hex and P-ALA-Hex to ALA-Hex by assessing the efficacy of the novel prodrugs to induce the formation of PpIX in five different cancer cell lines.

We also evaluated the cytotoxic effects of the prodrugs in the dark and upon the exposure to different light doses. Furthermore, we investigated the subcellular distribution of PpIX over time. The results show that all the cells used in this study are capable to produce PpIX after exposure to phosphatase-sensitive prodrugs.

Figures 3 and 4 demonstrate that the accumulation of PpIX is dependent on the prodrug used, its dose and the cell line. In general, the shape of dose-response curves for PSI-ALA-Hex and ALA-Hex is similar. Dose-response curve for P-ALA-Hex differs from the others in PC3, MCF7 and T24 cells since the PpIX accumulation still raises at 1 mM concentration of this phosphate-sensitive prodrug. In the case of PSI-ALA-Hex and ALA-Hex, PpIX accumulation decreases and is low at 1 mM concentration, probably due to unspecific cell toxicity, especially in the case of ALA-Hex (Figure S3). The optimal prodrug concentration differs from one cell line to the other probably due to different expression of enzymes needed for the transformation to 5-ALA. Overall, optimal concentration values for PSI-ALA-Hex and ALA-Hex are lower than for P-ALA-Hex. Altogether, the optimal concentration of PSI-ALA-Hex to induce the maximum PpIX production in cells can be compared to ALA-Hex and is between 0.03 and 0.33 mM. On the other hand, a higher dose than 1.00 mM of P-ALA-Hex is needed to induce the optimal cell response. This is most likely a consequence of different activation rates between the two phosphatase-sensitive prodrug classes needed for the conversion to 5-ALA.[21] The phenyl-phospho group of P-ALA-Hex is not an optimal substrate for alkaline phosphatases and has a very narrow concentration range for optimal activity hence the higher concentrations needed for activity.[33]

Furthermore, this study revealed that T24 and A549 cells produce significantly less PpIX in comparison to PC3 and MCF7 when exposed to 5-ALA prodrugs. Flow-cytometry PpIX normalized fluorescence intensities values at 4 h upon the incubation with 0.33 mM PSI-ALA-

Hex vary from 300 for T24 human bladder cancer and 160 for A549 lung adenocarcinoma to 3150 in the case of PC3 prostate cancer and 1200 for MCF7 breast adenocarcinoma cells (Figure S2). This provides good foundations for the diagnosis or treatment of prostate and breast cancer. Consequently, these findings explain lower efficacy of PDT in T24 and A549. It has been established that the efficacy of PDT is closely related to the amount of PpIX produced in cells, rather than the irradiation dose used.[34, 35] Moreover, Moan et al. showed that PpIX generation in cells is cell density and cell volume dependent being higher in G2 and M phase in comparison to G1.[36] Another explanation for the discrepancies in phototoxicity results between different cell lines may come from the fact that the photosensitivity of cells is larger in high-density cultures [36]. The low induction of PpIX production upon the incubation with phosphatase-sensitive prodrugs and not with the ALA-Hex in T24 cells might be due to the low expression levels of alkaline phosphatase previously reported in these cells.[37, 38] Also, T24 were initially plated in lower density possibly making them less photosensitive than the PC3 and MCF7 cells.

ALA-prodrug induced PpIX synthesis, accumulation and its subcellular localization are governed by several factors that differ between cell types. The first factor that has to be taken into consideration is the prodrug's uptake mechanism and the rate of uptake, followed by prodrug's metabolism which implicates the expression of different enzymes. Next, mitochondrial metabolic activity and the expression of porphyrin transporters like ABCB6 and ABCG2 has to be taken into consideration.[39-41] In spite of the fact that all cell lines used in our experiments are capable of PpIX production upon the incubation of different precursors namely, PSI-ALA-Hex, P-ALA-Hex and ALA-Hex, important differences can be seen in the quantity of PpIX produced depending on the cell line, type of precursor and its concentration. These results can be explained by the fact that each of the precursors used has a different metabolic rate to yield the 5-ALA which enters into the

heme cycle. While ALA-Hex, the esterase cleavage directly leads to 5-ALA formation, PSI-ALA-Hex and P-ALA-Hex are activated in several steps (Figure 2). Although abundantly present in tissues, the regulation of alkaline phosphatase expression changes due to different factors according to cell type.[24, 42, 43] It has to be noted that PSI-ALA-Hex upon activation gives rise to the production of formaldehyde. Although participating in fundamental biological pathways in cells, the excessive amounts of formaldehyde have toxic effects by inhibiting cell proliferation and leading to apoptosis through the upregulation of tumor suppressor genes p53 and p21 responsible for the cell cycle regulation.[44] Formaldehyde disposal from cells include its reduction to methanol via the cytosolic alcohol dehydrogenase (ADH) or by the oxidation to formate catalyzed by ADH3 in the cytosol or by aldehyde dehydrogenase (ALDH) in the mitochondria.[45-47] It has already been reported that formaldehyde forming prodrugs can have enhanced cytotoxic effects that are cell type dependent, prodrug concentration and the formaldehyde concentration dependent.[48] The latter may apply on the results obtained by monitoring the PpIX production in different cancer cell types (Figure 3, 4, S1 and S2).

Studies of subcellular localization of PpIX are important because ROS that are formed during the PDT have a very short half-life hence the mechanisms of action and effectiveness of PDT will depend on where in the cell the PpIX is located.[49] These findings may improve the current use of PDT and PD in clinics enabling personalized and more targeted cancer therapy and diagnoses. Our results are generally in agreement with previously reported studies of PpIX subcellular accumulation which demonstrate its dependence on the cell type used for the experiment.[40, 50, 51] Fluorescence images and the calculation of PCC indicate that PpIX accumulation is dependent on cell type but does not change for ALA-Hex and new 5-ALA derivatives, PSI-ALA-Hex and P-ALA-Hex. Different correlation values between PpIX fluorescence and mitochondria were

obtained for MCF7 and PC3 cells. In MCF7 cells, correlation between PpIX and mitochondria is low with no significant differences between different time points or drugs used. In PC3 cells, PCC is higher than in MCF7, but similarly, no major differences between different time points or PSI-ALA-Hex and ALA-Hex were observed.

Conclusions

All the assays preformed in this research are based on cell phenotype. We can argue that these results demonstrate diverse cellular responses to PpIX overproduction, its accumulation and induced dark- and phototoxicity upon the incubation with PSI-ALA-Hex and P-ALA-Hex. The novel phospho-double prodrugs of 5-ALA prodrugs induce the production PpIX in several cancer cell lines as demonstrated by fluorescence measurements of PpIX accumulation, flow cytometry and confocal fluorescence micrographs. Due to low dark- toxicity and good response to PDT, PSI-ALA-Hex and P-ALA-Hex present good candidates for further translational development of glioblastoma, breast and prostate cancer PD and PDT.

ASSOCIATED CONTENT

Supporting Information.

The Supporting Information is available free of charge at DOI:

AUTHOR INFORMATION

Corresponding Author

*E-mail: andrej.babic@unige.ch

Author Contributions

The manuscript was written through contributions of all authors. All authors have given approval to the final version of the manuscript.

Notes

The authors declare no competing financial interest.

ACKNOWLEDGEMENTS

We thank Cécile Gameiro from the Flow cytometry platform her help with flow cytometry experiments and Dr. Christoph Bauer and Jérôme Bosset from the Bioimaging platform at the University of Geneva for their input and help in live cell imaging. We are grateful to Dr. Laurence Marcourt of the School of Pharmaceutical Sciences Geneva-Lausanne for her contribution in NMR experiments. We would also like to acknowledge the Mass Spectrometry platform at the University of Geneva for the mass spectroscopy analysis. We thank Canton of Geneva, Switzerland and Swiss National Science Foundation for funding.

REFERENCES

1. Casas, A.; Perotti, C.; Ortel, B.; Di Venosa, G.; Saccoliti, M.; Batlle, A.; Hasan, T. Tumor cell lines resistant to ALA-mediated photodynamic therapy and possible tools to target surviving cells. *International journal of oncology* **2006,** *29*, (2), 397-405.
2. Dailey, H. A.; Smith, A. Differential interaction of porphyrins used in photoradiation therapy with ferrochelatase. *Biochem J* **1984,** *223*, (2), 441-5.
3. Kennedy, J. C.; Pottier, R. H. Endogenous Protoporphyrin-Ix, a Clinically Useful Photosensitizer for Photodynamic Therapy. *J Photoch Photobio B* **1992,** *14*, (4), 275-292.

4. Nguyen, Q. T.; Tsien, R. Y. Fluorescence-guided surgery with live molecular navigation - a new cutting edge. *Nat Rev Cancer* **2013,** *13*, (9), 653-662.
5. Peng, Q.; Warloe, T.; Berg, K.; Moan, J.; Kongshaug, M.; Giercksky, K. E.; Nesland, J. M. 5-Aminolevulinic acid-based photodynamic therapy. Clinical research and future challenges. *Cancer* **1997,** *79*, (12), 2282-308.
6. Brown, S. B.; Brown, E. A.; Walker, I. The present and future role of photodynamic therapy in cancer treatment. *The Lancet. Oncology* **2004,** *5*, (8), 497-508.
7. Jeffes, E. W.; McCullough, J. L.; Weinstein, G. D.; Fergin, P. E.; Nelson, J. S.; Shull, T. F.; Simpson, K. R.; Bukaty, L. M.; Hoffman, W. L.; Fong, N. L. Photodynamic therapy of actinic keratosis with topical 5-aminolevulinic acid. A pilot dose-ranging study. *Arch Dermatol* **1997,** *133*, (6), 727-32.
8. Dirschka, T.; Radny, P.; Dominicus, R.; Mensing, H.; Bruning, H.; Jenne, L.; Karl, L.; Sebastian, M.; Oster-Schmidt, C.; Klovekorn, W.; Reinhold, U.; Tanner, M.; Grone, D.; Deichmann, M.; Simon, M.; Hubinger, F.; Hofbauer, G.; Krahn-Senftleben, G.; Borrosch, F.; Reich, K.; Berking, C.; Wolf, P.; Lehmann, P.; Moers-Carpi, M.; Honigsmann, H.; Wernicke-Panten, K.; Helwig, C.; Foguet, M.; Schmitz, B.; Lubbert, H.; Szeimies, R. M.; Group, A.-C. S. Photodynamic therapy with BF-200 ALA for the treatment of actinic keratosis: results of a multicentre, randomized, observer-blind phase III study in comparison with a registered methyl-5-aminolaevulinate cream and placebo. *Br J Dermatol* **2012,** *166*, (1), 137-46.
9. Dirschka, T.; Radny, P.; Dominicus, R.; Mensing, H.; Bruning, H.; Jenne, L.; Karl, L.; Sebastian, M.; Oster-Schmidt, C.; Klovekorn, W.; Reinhold, U.; Tanner, M.; Grone, D.; Deichmann, M.; Simon, M.; Hubinger, F.; Hofbauer, G.; Krahn-Senftleben, G.; Borrosch, F.; Reich, K.; Berking, C.; Wolf, P.; Lehmann, P.; Moers-Carpi, M.; Honigsmann, H.; Wernicke-Panten, K.; Hahn, S.; Pabst, G.; Voss, D.; Foguet, M.; Schmitz, B.; Lubbert, H.; Szeimies, R. M.; Group, A.-C. S.; Group, A.-C. S. Long-term (6 and 12 months) follow-up of two prospective, randomized, controlled phase III trials of photodynamic therapy with BF-200 ALA and methyl aminolaevulinate for the treatment of actinic keratosis. *Br J Dermatol* **2013,** *168*, (4), 825-36.
10. Pariser, D. M.; Houlihan, A.; Ferdon, M. B.; Berg, J. E.; Group, P.-A. I. Randomized Vehicle-Controlled Study of Short Drug Incubation Aminolevulinic Acid Photodynamic Therapy for Actinic Keratoses of the Face or Scalp. *Dermatol Surg* **2016,** *42*, (3), 296-304.
11. Hefti, M.; Mehdorn, H. M.; Albert, I.; Dorner, L. Fluorescence-Guided Surgery for Malignant Glioma: A Review on Aminolevulinic Acid Induced Protoporphyrin IX Photodynamic Diagnostic in Brain Tumors. *Curr Med Imaging Rev* **2010,** *6*, (4), 254-258.
12. Stummer, W.; Pichlmeier, U.; Meinel, T.; Wiestler, O. D.; Zanella, F.; Reulen, H. J.; Group, A. L.-G. S. Fluorescence-guided surgery with 5-aminolevulinic acid for resection of malignant glioma: a randomised controlled multicentre phase III trial. *The Lancet. Oncology* **2006,** *7*, (5), 392-401.
13. Perotti, C.; Casas, A.; Fukuda, H.; Sacca, P.; Batlle, A. ALA and ALA hexyl ester induction of porphyrins after their systemic administration to tumour bearing mice. *Brit J Cancer* **2002,** *87*, (7), 790-795.
14. Gaullier, J. M.; Berg, K.; Peng, Q.; Anholt, H.; Selbo, P. K.; Ma, L. W.; Moan, J. Use of 5-aminolevulinic acid esters to improve photodynamic therapy on cells in culture. *Cancer Res* **1997,** *57*, (8), 1481-1486.
15. Foley, P. Clinical efficacy of methyl aminolevulinate (Metvix) photodynamic therapy. *J Dermatolog Treat* **2003,** *14 Suppl 3*, 15-22.

16. Lange, N.; Jichlinski, P.; Zellweger, M.; Forrer, M.; Marti, A.; Guillou, L.; Kucera, P.; Wagnieres, G.; van den Bergh, H. Photodetection of early human bladder cancer based on the fluorescence of 5-aminolaevulinic acid hexylester-induced protoporphyrin IX: a pilot study. *Br J Cancer* **1999,** *80*, (1-2), 185-93.
17. Fotinos, N.; Campo, M. A.; Popowycz, F.; Gurny, R.; Lange, N. 5-Aminolevulinic acid derivatives in photomedicine: Characteristics, application and perspectives. *Photochemistry and photobiology* **2006,** *82*, (4), 994-1015.
18. Lapini, A.; Minervini, A.; Masala, A.; Schips, L.; Pycha, A.; Cindolo, L.; Giannella, R.; Martini, T.; Vittori, G.; Zani, D.; Bellomo, F.; Cosciani Cunico, S. A comparison of hexaminolevulinate (Hexvix((R))) fluorescence cystoscopy and white-light cystoscopy for detection of bladder cancer: results of the HeRo observational study. *Surg Endosc* **2012,** *26*, (12), 3634-41.
19. Fradet, Y.; Grossman, H. B.; Gomella, L.; Lerner, S.; Cookson, M.; Albala, D.; Droller, M. J.; Group, P. B. S. A comparison of hexaminolevulinate fluorescence cystoscopy and white light cystoscopy for the detection of carcinoma in situ in patients with bladder cancer: a phase III, multicenter study. *J Urol* **2007,** *178*, (1), 68-73; discussion 73.
20. L'Eplattenier H, F.; Klem, B.; Teske, E.; van Sluijs, F. J.; van Nimwegen, S. A.; Kirpensteijn, J. Preliminary results of intraoperative photodynamic therapy with 5-aminolevulinic acid in dogs with prostate carcinoma. *Veterinary journal* **2008,** *178*, (2), 202-7.
21. Babic, A.; Herceg, V.; Ateb, I.; Allemann, E.; Lange, N. Tunable phosphatase-sensitive stable prodrugs of 5-aminolevulinic acid for tumor fluorescence photodetection. *Journal of controlled release : official journal of the Controlled Release Society* **2016,** *235*, 155-64.
22. Stebbing, J.; Lit, L. C.; Zhang, H.; Darrington, R. S.; Melaiu, O.; Rudraraju, B.; Giamas, G. The regulatory roles of phosphatases in cancer. *Oncogene* **2014,** *33*, (8), 939-53.
23. Benham, F. J.; Fogh, J.; Harris, H. Alkaline phosphatase expression in human cell lines derived from various malignancies. *International journal of cancer. Journal international du cancer* **1981,** *27*, (5), 637-44.
24. Dabare, A. A.; Nouri, A. M.; Cannell, H.; Moss, T.; Nigam, A. K.; Oliver, R. T. Profile of placental alkaline phosphatase expression in human malignancies: effect of tumour cell activation on alkaline phosphatase expression. *Urol Int* **1999,** *63*, (3), 168-74.
25. Yu, E. Y.; Saad, F.; Londhe, A.; Shore, N. D.; Van Poppel, H.; Rathkopf, D. E.; Smith, M. R.; Logothetis, C.; De Souza, P. L.; Fizazi, K.; Mulders, P. F. A.; Mainwaring, P. N.; Hainsworth, J. D.; Beer, T. M.; North, S. A.; Small, E. J.; Scher, H. I.; Griffin, T. W.; Yu, M. K.; Ryan, C. J. Association of alkaline phosphatase (ALP) with clinical outcomes in chemotherapy-naive patients (pts) with metastatic castration-resistant prostate cancer (mCRPC): Results from COU-AA-302. *Journal of Clinical Oncology* **2014,** *32*, (4).
26. Adler, J.; Parmryd, I. Quantifying colocalization by correlation: the Pearson correlation coefficient is superior to the Mander's overlap coefficient. *Cytometry A* **2010,** *77*, (8), 733-42.
27. Uehlinger, P.; Zellweger, M.; Wagnieres, G.; Juillerat-Jeanneret, L.; van den Bergh, H.; Lange, N. 5-Aminolevulinic acid and its derivatives: physical chemical properties and protoporphyrin IX formation in cultured cells. *Journal of photochemistry and photobiology. B, Biology* **2000,** *54*, (1), 72-80.
28. Lopez, R. F.; Lange, N.; Guy, R.; Bentley, M. V. Photodynamic therapy of skin cancer: controlled drug delivery of 5-ALA and its esters. *Advanced drug delivery reviews* **2004,** *56*, (1), 77-94.

29. Novo, M.; Huttmann, G.; Diddens, H. Chemical instability of 5-aminolevulinic acid used in the fluorescence diagnosis of bladder tumours. *Journal of photochemistry and photobiology. B, Biology* **1996,** *34*, (2-3), 143-8.
30. Butler, A. R.; George, S. The Nonenzymatic Cyclic Dimerization of 5-Aminolevulinic Acid. *Tetrahedron* **1992,** *48*, (37), 7879-7886.
31. Berger, Y.; Greppi, A.; Siri, O.; Neier, R.; Juillerat-Jeanneret, L. Ethylene glycol and amino acid derivatives of 5-aminolevulinic acid as new photosensitizing precursors of protoporphyrin IX in cells. *J Med Chem* **2000,** *43*, (25), 4738-4746.
32. Giuntini, F.; Bourre, L.; MacRobert, A. J.; Wilson, M.; Eggleston, I. M. Improved Peptide Prodrugs of 5-ALA for PDT: Rationalization of Cellular Accumulation and Protoporphyrin IX Production by Direct Determination of Cellular Prodrug Uptake and Prodrug Metabolization. *J Med Chem* **2009,** *52*, (13), 4026-4037.
33. Morton, R. K. The kinetics of hydrolysis of phenyl phosphate by alkaline phosphatases. *Biochem J* **1957,** *65*, (4), 674-82.
34. Lee, J. B.; Choi, J. Y.; Chun, J. S.; Yun, S. J.; Lee, S. C.; Oh, J.; Park, H. R. Relationship of protoporphyrin IX synthesis to photodynamic effects by 5-aminolaevulinic acid and its esters on various cell lines derived from the skin. *Br J Dermatol* **2008,** *159*, (1), 61-7.
35. Chen, R.; Huang, Z.; Chen, G.; Li, Y.; Chen, X.; Chen, J.; Zeng, H. Kinetics and subcellular localization of 5-ALA-induced PpIX in DHL cells via two-photon excitation fluorescence microscopy. *International journal of oncology* **2008,** *32*, (4), 861-7.
36. Moan, J.; Bech, O.; Gaullier, J. M.; Stokke, T.; Steen, H. B.; Ma, L. W.; Berg, K. Protoporphyrin IX accumulation in cells treated with 5-aminolevulinic acid: dependence on cell density, cell size and cell cycle. *International journal of cancer. Journal international du cancer* **1998,** *75*, (1), 134-9.
37. Herz, F.; Barlebo, H.; Koss, L. G. Modulation of alkaline phosphatase activity in cell cultures derived from human urinary bladder carcinoma. *Cancer Res* **1974,** *34*, (8), 1943-6.
38. Benham, F.; Cottell, D. C.; Franks, L. M.; Wilson, P. D. Alkaline phosphatase activity in human bladder tumor cell lines. *J Histochem Cytochem* **1977,** *25*, (4), 266-74.
39. Yang, X.; Palasuberniam, P.; Kraus, D.; Chen, B. Aminolevulinic Acid-Based Tumor Detection and Therapy: Molecular Mechanisms and Strategies for Enhancement. *Int J Mol Sci* **2015,** *16*, (10), 25865-80.
40. Palasuberniam, P.; Yang, X.; Kraus, D.; Jones, P.; Myers, K. A.; Chen, B. ABCG2 transporter inhibitor restores the sensitivity of triple negative breast cancer cells to aminolevulinic acid-mediated photodynamic therapy. *Sci Rep* **2015,** *5*, 13298.
41. Khan, A. A.; Quigley, J. G. Control of intracellular heme levels: heme transporters and heme oxygenases. *Biochimica et biophysica acta* **2011,** *1813*, (5), 668-82.
42. Stefkova, K.; Prochazkova, J.; Pachernik, J. Alkaline phosphatase in stem cells. *Stem Cells Int* **2015,** *2015*, 628368.
43. Tsai, L. C.; Hung, M. W.; Chen, Y. H.; Su, W. C.; Chang, G. G.; Chang, T. C. Expression and regulation of alkaline phosphatases in human breast cancer MCF-7 cells. *Eur J Biochem* **2000,** *267*, (5), 1330-9.
44. Nudelman, A.; Levovich, I.; Cutts, S. M.; Phillips, D. R.; Rephaeli, A. The role of intracellularly released formaldehyde and butyric acid in the anticancer activity of acyloxyalkyl esters. *J Med Chem* **2005,** *48*, (4), 1042-54.

45. Friedenson, B. A common environmental carcinogen unduly affects carriers of cancer mutations: carriers of genetic mutations in a specific protective response are more susceptible to an environmental carcinogen. *Med Hypotheses* **2011,** *77*, (5), 791-7.
46. MacAllister, S. L.; Choi, J.; Dedina, L.; O'Brien, P. J. Metabolic mechanisms of methanol/formaldehyde in isolated rat hepatocytes: carbonyl-metabolizing enzymes versus oxidative stress. *Chem Biol Interact* **2011,** *191*, (1-3), 308-14.
47. Tulpule, K.; Hohnholt, M. C.; Dringen, R. Formaldehyde metabolism and formaldehyde-induced stimulation of lactate production and glutathione export in cultured neurons. *J Neurochem* **2013,** *125*, (2), 260-72.
48. Levovich, I.; Nudelman, A.; Berkovitch, G.; Swift, L. P.; Cutts, S. M.; Phillips, D. R.; Rephaeli, A. Formaldehyde-releasing prodrugs specifically affect cancer cells by depletion of intracellular glutathione and augmentation of reactive oxygen species. *Cancer Chemother Pharmacol* **2008,** *62*, (3), 471-82.
49. Postiglione, I.; Barra, F.; Aloj, S. M.; Palumbo, G. Photodynamic therapy with 5-aminolaevulinic acid and DNA damage: unravelling roles of p53 and ABCG2. *Cell Prolif* **2016,** *49*, (4), 523-38.
50. Wang, H.; Yang, Y.; Chen, H.; Dan, J.; Cheng, J.; Guo, S.; Sun, X.; Wang, W.; Ai, Y.; Li, S.; Li, Z.; Peng, L.; Tian, Z.; Yang, L.; Wu, J.; Zhong, X.; Zhou, Q.; Wang, P.; Zhang, Z.; Cao, W.; Tian, Y. The predominant pathway of apoptosis in THP-1 macrophage-derived foam cells induced by 5-aminolevulinic acid-mediated sonodynamic therapy is the mitochondria-caspase pathway despite the participation of endoplasmic reticulum stress. *Cell Physiol Biochem* **2014,** *33*, (6), 1789-801.
51. Liang, H.; Shin, D. S.; Lee, Y. E.; Nguyen, D. C.; Trang, T. C.; Pan, A. H.; Huang, S. L.; Chong, D. H.; Berns, M. W. Subcellular phototoxicity of 5-aminolaevulinic acid (ALA). *Lasers Surg Med* **1998,** *22*, (1), 14-24.